HHS Public Access

Author manuscript

*Abdom Radiol (NY)*. Author manuscript; available in PMC 2021 August 01.

Published in final edited form as:

*Abdom Radiol (NY)*. 2021 August ; 46(8): 3927–3934. doi:10.1007/s00261-021-03073-0.

# Assessment of agreement between manual and automated processing of liver MR elastography for shear stiffness estimation in children and young adults with autoimmune liver disease

**Deep B. Gandhi**[1], **Amol Pednekar**[2,3,9], **Adebayo B. Braimah**[1], **Jonathan Dudley**[1], **Jean A. Tkach**[2,3], **Andrew T. Trout**[2,3,4], **Alexander G. Miethke**[4,5], **Marnix D. Franck**[2,6], **Jeremiah A. Heilman**[7], **Bogdan Dzyubak**[8], **David S. Lake**[8], **Jonathan R. Dillman**[1,2,3]

[1]Department of Radiology, Imaging Research Center (IRC), Cincinnati Children's Hospital Medical Center (CCHMC), Cincinnati, OH, USA [2]Department of Radiology, Cincinnati Children's Hospital Medical Center, Cincinnati, OH, USA [3]Department of Radiology, University of Cincinnati College of Medicine, Cincinnati, OH, USA [4]Department of Pediatrics, University of Cincinnati College of Medicine, Cincinnati, OH, USA [5]Division of Hepatology, Gastroenterology and Nutrition, Cincinnati Children's Hospital Medical Center (CCHMC), Cincinnati, OH, USA [6]Radboud University, Nijmegen, The Netherlands [7]Resoundant, Inc., Rochester, MN, USA [8]Department of Radiology, Mayo Clinic, Rochester, MN, USA [9]Imaging Research Center, 3333 Burnet Avenue, Suite S1.533, Cincinnati, OH 45229, USA

## Abstract

**Purpose—**To compare automated versus standard of care manual processing of 2D gradient recalled echo (GRE) liver MR Elastography (MRE) in children and young adults.

**Materials and methods—**2D GRE liver MRE data from research liver MRI examinations performed as part of an autoimmune liver disease registry between March 2017 and March 2020 were analyzed retrospectively. All liver MRE data were acquired at 1.5 T with 60 Hz mechanical vibration frequency. For manual processing, two independent readers (R1, R2) traced regions of interest on scanner generated shear stiffness maps. Automated processing was performed using MREplus+ (Resoundant Inc.) using 90% (A90) and 95% (A95) confidence masks. Agreement was evaluated using intra-class correlation coefficients (ICC) and Bland–Altman analyses. Classification performance was evaluated using receiver operating characteristic curve (ROC) analyses.

**Results—**In 65 patients with mean age of 15.5 ± 3.8 years (range 8–23 years; 35 males) median liver shear stiffness was 2.99 kPa (mean 3.55 ± 1.69 kPa). Inter-reader agreement for manual processing was very strong (ICC = 0.99, mean bias = 0.01 kPa [95% limits of agreement (LoA): − 0.41 to 0.44 kPa]). Correlation between manual and A95 automated processing was very strong (R1: ICC = 0.988, mean bias = 0.13 kPa [95% LoA: − 0.40 to 0.68 kPa]; R2: ICC = 0.987, mean

✉Amol Pednekar, Amol.Pednekar@cchmc.org.

bias = 0.13 kPa [95% LoA: − 0.44 to 0.69 kPa]). Automated measurements were perfectly replicable (ICC = 1.0; mean bias = 0 kPa).

**Conclusion—**Liver shear stiffness values obtained using automated processing showed excellent agreement with manual processing. Automated processing of liver MRE was perfectly replicable.

### Keywords

Magnetic resonance elastography (MRE); Pediatric; Liver; Shear stiffness; Automated region of interest

## Introduction

Quantification of liver shear stiffness is important for diagnosis, stratification, and monitoring of diffuse liver diseases, particularly those that result in excessive accumulation of extracellular matrix and collagen. Magnetic resonance elastography (MRE) of the liver, a United States Food and Drug Administration (FDA)-approved clinical tool, has been shown to aid in the non-invasive diagnosis and staging of liver fibrosis [1–5]. There is a substantial body of literature regarding the use of liver MRE in adult populations, and a growing body of pediatric literature, including published data on the normal range for liver shear stiffness in children without liver disease [6, 7].

For current standard of care liver MRE on 1.5 T scanners, four transverse 2D gradient recalled echo (GRE) slices are acquired through the mid liver with synchronized 60 Hz mechanical vibrations. In clinical practice, these liver MRE images are converted into shear stiffness maps using multi modal direct inversion (MMDI) on the scanner along with the overlay of 95% confidence masks computed as the fit of a smooth polynomial to the phase images [8]. An experienced reader then manually draws region of interests (ROI) on these shear stiffness maps within the area bounded by the confidence maps, avoiding edges of liver parenchyma, large blood vessels, dilated bile ducts, and artifacts. This manual contouring of irregularly shaped ROIs is a time-consuming process, requiring up to 10 min per patient. Additionally, this process is subjective, with previous studies reporting inter-reader variability in measured stiffness of 7 ± 23% [9].

An automated post-processing tool that was developed/designed to delineate liver tissue in regions of confidence interval greater than the specified threshold (90% or 95%) and report the associated shear stiffness values holds promise to provide a substantial improvement in workflow and to facilitate standardization of clinical and research liver MRE assessments of liver shear stiffness. Previously published studies using automated liver MRE analysis for assessment in adults has shown great promise [7, 10] but there is little data in general and essentially no data in the pediatric autoimmune liver disease population. Therefore, the purpose of our study was to compare automated computer-derived 2D GRE liver MRE measurements against standard manual processing in children and young adults.

## Methods

This HIPAA-compliant study analyzed research MRI data acquired under an Institutional Review Board (IRB) approved study of autoimmune liver disease. Written informed consent had been obtained from participants (or guardian caretakers where applicable).

### Patients

We identified all patients who had undergone liver MRE as part of a baseline research MRI for autoimmune liver disease (sclerosing cholangitis, autoimmune sclerosing cholangitis and autoimmune hepatitis) registry participation between March 2017 and March 2020.

### MR image acquisition

All patients fasted for a minimum of 4 h prior to research imaging. All liver MRE examinations were acquired on a single 1.5 T clinical MR scanner (Ingenia; Philips Healthcare; Best, the Netherlands) using a 2D GRE MRE sequence, 28-element anterior torso coil, and 60 Hz mechanical vibration. The amplitude of the active driver was chosen based on the body habitus of the subjects (varied between 30 and 70% of the maximum amplitude). Liver MRE was performed in supine head-first position with four 10-mm thick axial images acquired through the mid liver. Each image was obtained during a 13-s breath hold [11]. Imaging parameters for the clinical 2D GRE MRE sequence included: echo time (TE) = 20 ms, time of repetition (TR) = 50 ms, flip angle = 20°, sensitivity encoding (SENSE) acceleration factor = 2, acquisition matrix = 252 × 80 (reconstructed to 350 × 350), and field of view (FOV) = 380 × 380 mm (kept constant in all subjects for consistency), 4 time offsets, and superior and inferior saturation bands to suppress flow artifacts. Motion encoding gradients were zero- and first-moment compensated with 1-2-1 trapezoidal gradient wave-forms and applied in the foot to head direction.

All the liver MRE data, including magnitude, phase, and wave images as well as shear stiffness maps, were exported to post-processing workstations in standard DICOM format.

### Generation of shear stiffness maps

For generation of standard of care images for manual analysis, shear stiffness maps and 95% confidence masks were generated by the scanner software per routine clinical protocol. For automated analysis, shear stiffness maps and confidence masks were generated by the investigational offline analysis program during the process of analysis. Both the scanner software, as well as the automated analysis program, used a MMDI algorithm for computation of shear stiffness maps and associated confidence masks by calculating the quality of fit of low order polynomials to the wave data [12].

### Image analysis

Manual liver shear stiffness measurements were made using commercially available FDA-approved software (IntelliSpace Portal v10.1; ISP, Philips Healthcare). Manual measurements were made by two trained image analysts (R1 with more than one-year experience, and R2 with 2 months of experience in liver MRE processing), under the supervision of a board-certified Pediatric Radiologist with greater than 10 years post-

fellowship experience who reviewed all measurements (J.R.D). The two readers were blinded to each other's analysis and to the automated analysis results. As in clinical practice, a single irregular freehand ROI was drawn on each of the four axial images to encompass as much of the right hepatic lobe as possible while remaining within the boundaries of the 95% confidence mask and avoiding the liver capsule, large blood vessels, dilated bile ducts, and areas of artifact such as hot spots under the passive driver and respiratory motion in cases of failed breath holds (Fig. 1). Artifact was identified by direct inspection of source liver MRE images.

Automated liver shear stiffness measurements were made using an investigational program (MREplus+, Resoundant Inc., Rochester, MN) that generated shear stiffness maps and ROIs based on automatic liver segmentation from magnitude and phase data [12]. The automated algorithm uses relative spatial positions and intensities for initial estimation of the spatial location and extent of liver, fat, and background, followed by 2D segmentation to calculate a liver mask from MRE magnitude images. The algorithm identifies the areas with high contrast in magnitude images and sharp perturbations in the wave images, and then evaluates the elasticity to exclude any artifacts [12]. Finally, a confidence mask with a prescribed cutoff of 90% or 95% is applied to remove areas with low signal-to-noise wave data, and the mean liver shear stiffness is calculated from the resulting ROIs.

The liver MRE DICOM images for all the exams evaluated for this study were processed by the automated technique in a single batch processing session absent any user intervention (Fig. 1). The batch MRE processing was performed twice, first with a 90% confidence mask since it is the standard setting for the automated program and second time with 95% confidence mask to match our clinical processing. Analyses were fully automatic; no manual input to the Liver MRE data was required. All the ROIs from automated analyses were manually checked and no ROIs were observed in the non-liver region. The time required for manual and automated liver MRE set-up and processing was tracked and reported.

## Repeatability analysis

The automated batch processing was repeated after one month for both 90% and 95% confidence masks to assess repeatability. To assess intra-reader repeatability, one year after drawing the first set of manual contours, R1 redrew manual ROIs on 20 randomly chosen datasets using proportionate stratified sampling in groups of < 2 kPa, 2–3 kPa, 3–4 kPa, 4–5 kPa, and > 5 kPa.

To confirm that the different processing pathways (MMDI on the scanner, MMDI within the automated technique) did not introduce differences in measured liver stiffness, R1 drew simplified, identically sized and positioned ROIs on both sets of shear stiffness maps.

## Calculation of liver shear stiffness

Overall patient-specific liver shear stiffness was calculated as the area weighted mean liver shear stiffness from the four liver MRE slices to account for variation in ROI size.

### Statistical analysis

Two-sided paired *t* test, Bland–Altman analysis, and intra-class correlation (ICC) were used to compare and assess agreement in the ROI size and shear stiffness measurements within and between manual (R1 and R2) and automated (A90 and A95) processing. Reference true negative (suggestive of Ludwig stage 0–1) and true positive (suggestive of Ludwig stage 2 or higher) categorical classifications for liver fibrosis were assigned based on manual measurements performed by R1 and a previously published optimal stiffness cutoff value of 2.27 kPa (based on estimated liver shear stiffness data measured via a manual processing approach) for this distinction [13]. Classification performance of each processing method was then compared to this reference classification using receiver operating characteristic curve (ROC) analysis. Optimal stiffness cutoff values, maximizing both sensitivity and specificity, were calculated for R2, A90, and A95 and sensitivity, specificity, positive predictive value, negative predictive value, and total accuracy were calculated.

A $p$ value < 0.05 was considered significant for all inference testing and 95% confidence intervals were calculated as appropriate. Correlation coefficients were interpreted as follows: 0–0.19, very weak; 0.2–0.39, weak; 0.40–0.59, moderate; 0.60–0.79, strong; and 0.80–1.0, very strong [14]. All statistical analyses were performed using MATLAB (The MathWorks™ Inc., Natick, Massachusetts, USA).

## Results

Sixty-five patients underwent 2D GRE liver MRE during the study period, 35 males and 30 females, with a mean age of 15.5 ± 3.8 years (range 8–23 years). All MRE data were analyzed successfully, both manually and automatically. Manual processing required a mean of 6 ± 1 min per patient, for a total analysis time of 6 h and 30 min per reader for 65 patients. The same 2D GRE liver MRE data were processed automatically by the automated technique in the background using a batch file in MATLAB (The MathWorks™ Inc., Natick, Massachusetts, USA), which required 3 min and 30 s to set up. Mean computation time for each patient using the automated processing was 2 min and 50 s on a Microsoft Windows 10 system with Intel® Core ™ i5–7500, 4 Core CPU, and 16 GB RAM, resulting in a total processing time of 3 h and 8 min. Representative images with manual and automated analysis over a range of shear stiffness values are depicted in Fig. 1.

Area weighted mean liver shear stiffness values measured by R1 and R2 ranged from 1.66 to 9.45 kPa (median 2.99 kPa, mean 3.55 kPa, standard deviation 1.69 kPa). Area weighted mean liver shear stiffness values measured by the automated technique ranged from 1.54 to 8.77 kPa (median 2.70 kPa, mean 3.30 kPa, standard deviation 1.63 kPa) for data with a 90% confidence mask and 1.53 to 9.66 kPa (median 2.80 kPa, mean 3.42 kPa, standard deviation 1.74 kPa) for data with a 95% confidence mask. Total area size of the ROIs per patient measured by R1 and R2 ranged from 3687 to 24,646 $mm^2$ (median 9077 $mm^2$, mean 9979 $mm^2$, standard deviation 4032 $mm^2$). Total area size of the ROIs per patient measured by the automated technique ranged from 3424 to 21,780 $mm^2$ (median 11,018 $mm^2$, mean 11,746 $mm^2$, standard deviation 4630 $mm^2$) for data with a 90% confidence mask and 1465 to 16,726 $mm^2$ (median 7999 $mm^2$, mean 8524 $mm^2$, standard deviation 3679 $mm^2$) for data with a 95% confidence mask.

Agreement between liver shear stiffness measurements made by R1, R2 and the automated technique are presented in Table 1. Bland–Altman analysis and scatter plots are presented in Figs. 2 and 3. The absolute agreement between shear stiffness measurements made by each of the methods was very strong (ICCs > 0.98). Linear least squares regression on differences indicated no (p = 0.223) to negligible (< 1%, $p < 0.001$) proportional bias between methods. Intra-reader (bias 0.04 kPa (1.8%), $p = 0.23$) and inter-reader (bias 0.01 kPa (0.58%), $p = 0.66$) liver shear stiffness values were similar. Automatically computed liver shear stiffness values measured using a 90% confidence mask were statistically significantly underestimated (bias 0.13 kPa, 3.24%, $p < 0.001$) compared to automatically computed liver shear stiffness values with a 95% confidence mask.

A95 liver shear stiffness values were statistically significantly underestimated compared to both R1 (bias 0.14 kPa (4.8%), p < 0.001) and R2 (bias 0.13 kPa (4.2%), $p < 0.001$). The biases for liver shear stiffness values between A90 and manual methods (R1-A90 0.26 kPa (8.12%), R2-A90 0.27 kPa (7.76%)) were equal to the sum of the bias between A90 and A95 and the bias between manual and A95 processing.

Agreement in shear stiffness values between scanner and the automated program generated stiffness maps with simplified identical ROIs (ICC = 0.999) was very strong. Liver stiffness values computed by repeat A95 batch processing with the automated technique were perfectly reproducible (ICC = 1.0).

## Regions of interest

R1's initial and repeat ROI sizes showed very strong repeatability (ICC = 0.86), while the agreement between R1's and R2's ROI sizes (ICC = 0.62) was moderate to strong (Table 2). The difference in liver shear stiffness measurements for R1's repeat measurements ($r = -0.62$, $p < 0.0001$) and between R1 and R2 ($r = -0.57$, $p < 0.0001$) was moderately associated with differences in ROI sizes.

Agreement of ROI sizes between A95 and A90 automated analysis was moderate to strong (ICC = 0.61). The difference in liver shear stiffness measurements between A95 and A90 was very weakly associated with difference in ROI sizes ($r = -0.21$, $p = 0.0012$).

Agreement of ROI sizes between manual and automated methods was moderate (R1-A95 ICC = 0.497, R1-A90 ICC = 0.471) to weak (R2-A95 ICC = 0.314, R2-A90 ICC = 0.312). The differences in liver shear stiffness measurements between manual and automated methods were weakly associated with difference in ROI size ($r < -0.35$, $p < 0.0001$).

## Fibrosis classification performance

Results of categorical liver fibrosis classification performance for shear stiffness values measured by R2 and by the automated technique, relative to R1 as a reference standard using a threshold of 2.27 kPa are presented in Table 3. The false negative rates for R2, A95, and A90 were 1.92%, 13.46%, and 11.54% respectively. Sensitivity and specificity were maximized for A95 at 94.23% and 92.31%, respectively at cutoff value of 2.21 kPa, and for A90 at 98.08% and 100%, respectively at a cutoff value of 2.08 kPa.

## Discussion

Our results show very strong agreement (ICC > 0.98) between manual and automated area weighted liver MRE liver shear stiffness measurements. Liver stiffness values from the automated method were slightly but significantly ($p < 0.001$) underestimated compared to manual processing by less than 0.15 kPa (5%) with A95 and less than 0.3 kPa (8%) with A90. This bias is of negligible clinical significance and optimal stiffness cutoff values for A90 had very high accuracy (98%) for shear stiffness-based classification of Ludwig stage 0–1 versus stage 2 or higher liver fibrosis.

The inter and intra-reader liver stiffness bias and limits of agreement for manual processing in our study were similar to those previously reported for agreement between two different experienced centers [7]. In our study, liver stiffness underestimation bias between A95 and manual processing [0.13 kPa (R1 and R2)] was twice that reported in previous study (0.07 kPa) and the standard deviation of the difference (0.28 kPa vs. 0.3 kPa) was similar [15].

Importantly, the observed bias between manual and automated processing does not appear to relate to the process of generation of shear stiffness maps, but instead due to a combination of differences in ROI size, shape, and positioning. While there was weak correlation between differences in ROI size and differences in shear stiffness values between manual and automated methods, the bulk of the bias in shear stiffness appears to relate to the shape and spatial location of the ROIs. Specifically, in accordance with our clinical practice, manual contours drawn by both the readers were a single contiguous ROI strictly confined to the right lobe, while the automated contours could consist of multiple discontinuous ROIs and could extend into the left lobe of the liver. Based on the visual inspection of the ROIs, in 41.5% (27/65) of the patients automated ROIs with 90% confidence extended to deeper structures and 51.8% (14/27) of those cases with extended ROIs had lower stiffness measurements. Further, independent of the confidence mask, the automated contour detection algorithm conservatively excluded potentially partial volumed pixels at the outer boundaries of the liver.

In addition to showing minimal absolute bias relative to manual techniques, when referenced to the published threshold of 2.27 kPa for identification of abnormal liver stiffness in children, shear stiffness cutoff values of the automated method run with two different thresholds roughly corresponded to the published reference value adjusted by/for the threshold’s respective estimated bias. This suggests preserved discriminatory accuracy for the presence of abnormal liver stiffening in children across processing methods.

Automated analysis has several advantages over manual analysis. First, our results suggest measured liver stiffness is perfectly reproducible when analyzed automatically. Second, while there is a time requirement for batch set-up, the overall set-up and automated liver MRE processing time is still shorter than that required for manual processing and the automated system is capable of processing large numbers of examinations. Third, automated analysis requires little human input, appreciably reducing the need for personnel to do this work.

There are a few limitations to this study. First, the study population was an older pediatric and young adult autoimmune liver disease population. Thus, agreement of the two analysis methods in younger children (< 8 years old) and across a wide range of liver disease etiology has not been assessed. However, there is nothing unique/specific to the analysis methods that would suggest different performance in other populations. Second, the 2D GRE liver MRE data evaluated were acquired exclusively on one 1.5 T MR scanner manufactured by a single vendor. Performance of the automated analysis on liver MRE data acquired across MR scanner vendor platforms, at both 1.5 T and 3 T, as well as using spin echo-echo planar imaging sequences remains to be assessed. Similarly, the impact of the presence of potentially confounding pathologic conditions (comorbidities) such as hepatic iron loading on performance also needs to be explored.

## Conclusion

Liver MRE liver shear stiffness values computed/measured using a computer-based automated method showed excellent agreement with manual analysis and was perfectly replicable with maintained classification performance for Ludwig stage 0–1 versus Ludwig stage ≥ 2 fibrosis.

## Funding

This work was not funded by a grant or any other source of external funding.

## References

1. Yin M, Talwalkar JA, Glaser KJ, Manduca A, Grimm RC, Rossman PJ, Fidler JL, Ehman RL. Assessment of hepatic fibrosis with magnetic resonance elastography. Clinical gastroenterology and hepatology : the official clinical practice journal of the American Gastroenterological Association 2007;5(10):1207–1213.e1202. 10.1016/j.cgh.2007.06.012 [PubMed: 17916548]
2. Huwart L, Sempoux C, Vicaut E, Salameh N, Annet L, Danse E, Peeters F, ter Beek LC, Rahier J, Sinkus R, Horsmans Y, Van Beers BE. Magnetic resonance elastography for the noninvasive staging of liver fibrosis. Gastroenterology 2008;135(1):32–40. 10.1053/j.gastro.2008.03.076 [PubMed: 18471441]
3. Venkatesh SK, Yin M, Ehman RL. Magnetic resonance elastography of liver: technique, analysis, and clinical applications. Journal of magnetic resonance imaging : JMRI 2013;37(3):544–555. 10.1002/jmri.23731 [PubMed: 23423795]
4. Xanthakos SA, Podberesky DJ, Serai SD, Miles L, King EC, Balistreri WF, Kohli R. Use of magnetic resonance elastography to assess hepatic fibrosis in children with chronic liver disease. J Pediatr 2014;164(1):186–188. 10.1016/j.jpeds.2013.07.050 [PubMed: 24064151]
5. Singh S, Venkatesh SK, Wang Z, Miller FH, Motosugi U, Low RN, Hassanein T, Asbach P, Godfrey EM, Yin M, Chen J, Keaveny AP, Bridges M, Bohte A, Murad MH, Lomas DJ, Talwalkar JA, Ehman RL. Diagnostic performance of magnetic resonance elastography in staging liver fibrosis: a systematic review and meta-analysis of individual participant data. Clinical gastroenterology and hepatology : the official clinical practice journal of the American Gastroenterological Association 2015;13(3):440–451. e446. 10.1016/j.cgh.2014.09.046 [PubMed: 25305349]
6. Trout AT, Anupindi SA, Gee MS, Khanna G, Xanthakos SA, Serai SD, Baikpour M, Calle-Toro JS, Ozturk A, Zhang B, Dillman JR. Normal Liver Stiffness Measured with MR Elastography in Children. Radiology 2020:201513. 10.1148/radiol.2020201513
7. Sawh MC, Newton KP, Goyal NP, Angeles JE, Harlow K, Bross C, Schlein AN, Hooker JC, Sy EZ, Glaser KJ, Yin M, Ehman RL, Sirlin CB, Schwimmer JB. Normal range for MR elastography

measured liver stiffness in children without liver diseas. Journal of Magnetic Resonance Imaging 2020;51(3):919–927. 10.1002/JMRI.26905 [PubMed: 31452280]

8. Venkatesh SK, Ehman RL. Magnetic resonance elastography of abdomen. Abdom Imaging 2015;40(4):745–759. 10.1007/s00261-014-0315-6 [PubMed: 25488346]
9. Dzyubak B, Glaser K, Yin M, Talwalkar J, Chen J, Manduca A, Ehman RL. Automated liver stiffness measurements with magnetic resonance elastography. Journal of Magnetic Resonance Imaging 2013;38(2):371–379. 10.1002/jmri.23980 [PubMed: 23281171]
10. Hoodeshenas S, Welle CL, Navin PJ, Dzyubak B, Eaton JE, Ehman RL, Venkatesh SK. Magnetic Resonance Elastography in Primary Sclerosing Cholangitis: Interobserver Agreement for Liver Stiffness Measurement with Manual and Automated Methods. Academic Radiology 2019;26(12):1625–1632. 10.1016/j.acra.2019.02.004 [PubMed: 30878345]
11. Joshi M, Dillman J, Towbin A, Serai S, Trout A. MR elastography: high rate of technical success in pediatric and young adult patients. Pediatric Radiology 2017;47:838–343. 10.1007/s00247-017-3831-z [PubMed: 28367603]
12. Dzyubak B, Venkatesh SK, Manduca A, Glaser KJ, Ehman RL. Automated liver elasticity calculation for MR elastography. Journal of Magnetic Resonance Imaging 2016;43(5):1055–1063. 10.1002/jmri.25072 [PubMed: 26494224]
13. Trout AT, Sheridan RM, Serai SD, Xanthakos SA, Su W, Zhang B, Wallihan DB. Diagnostic Performance of MR Elastography for Liver Fibrosis in Children and Young Adults with a Spectrum of Liver Diseases. Radiology 2018;287(3):824–832. 10.1148/radiol.2018172099 [PubMed: 29470938]
14. Wuensch K, Evans J. Straightforward Statistics for the Behavioral Sciences. . Journal of the American Statistical Association 1996;91(436). 10.2307/2291607
15. Schwimmer JB, Behling C, Angeles JE, Paiz M, Durelle J, Africa J, Newton KP, Brunt EM, Lavine JE, Abrams SH, Masand P, Krishnamurthy R, Wong K, Ehman RL, Yin M, Glaser KJ, Dzyubak B, Wolfson T, Gamst AC, Hooker J, Haufe W, Schlein A, Hamilton G, Middleton MS, Sirlin CB. Magnetic resonance elastography measured shear stiffness as a biomarker of fibrosis in pediatric nonalcoholic fatty liver disease. Hepatology (Baltimore, Md) 2017;66(5):1474–1485. 10.1002/hep.29241

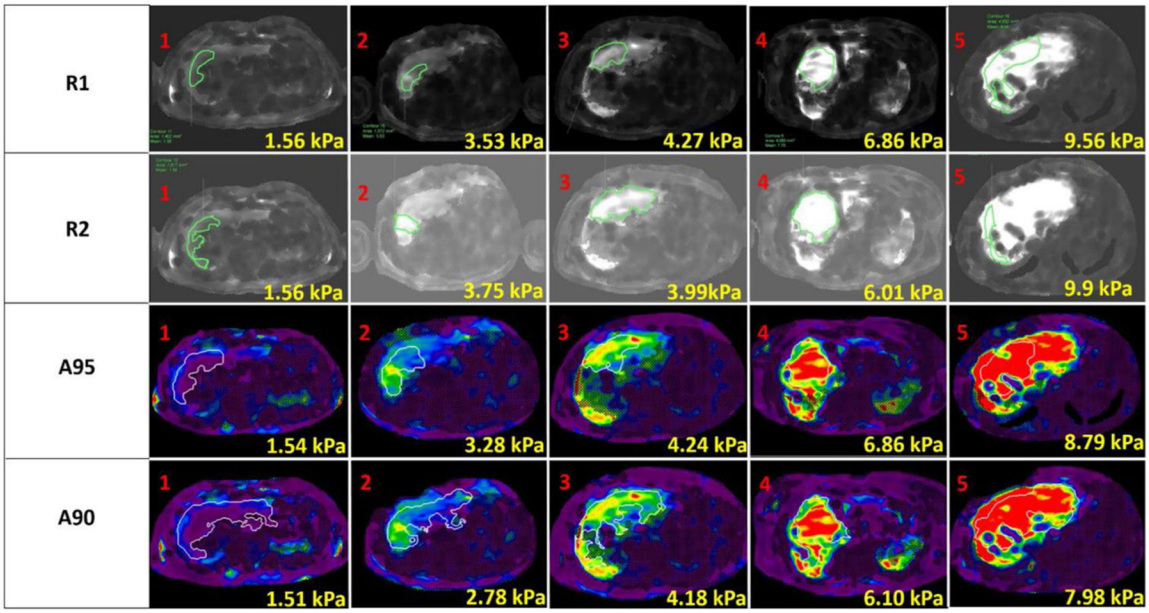


**Fig. 1.**

Representative magnetic resonance elastography-based shear stiffness maps generated in 5 patients (columns) with overlaid ROIs from manual and automated processing. The associated mean shear stiffness values for the contoured ROI are presented on the individual images

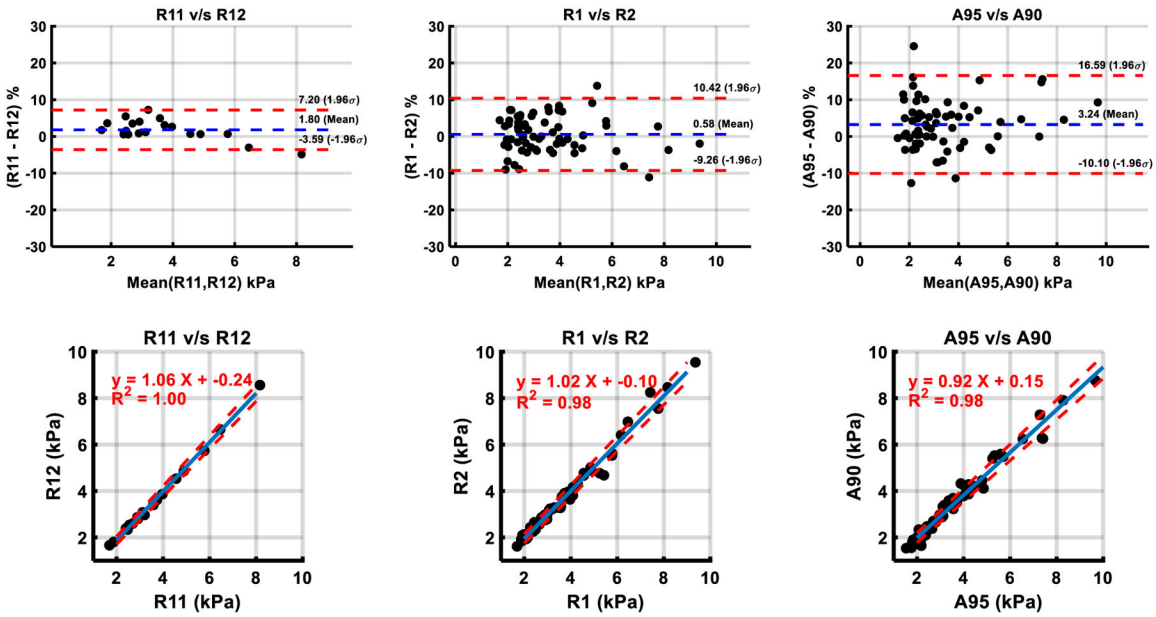


**Fig. 2.**

Comparison of shear stiffness measurements within manual and automated methods by Bland–Altman analysis and Linear Regression. Manual analysis informed by a 95% confidence mask by Reader 1 (R1) and Reader 2 (R2). Automated analysis using a 95% confidence mask (A95) and a 90% confidence mask (A90). Intra-reader comparison for a 95% confidence mask in 20 subjects using Reader 1's initial set of contours (R1,1) and his repeat contours (R1,2). In scatter plots, blue line—list squares fit, dotted red line—95% confidence interval

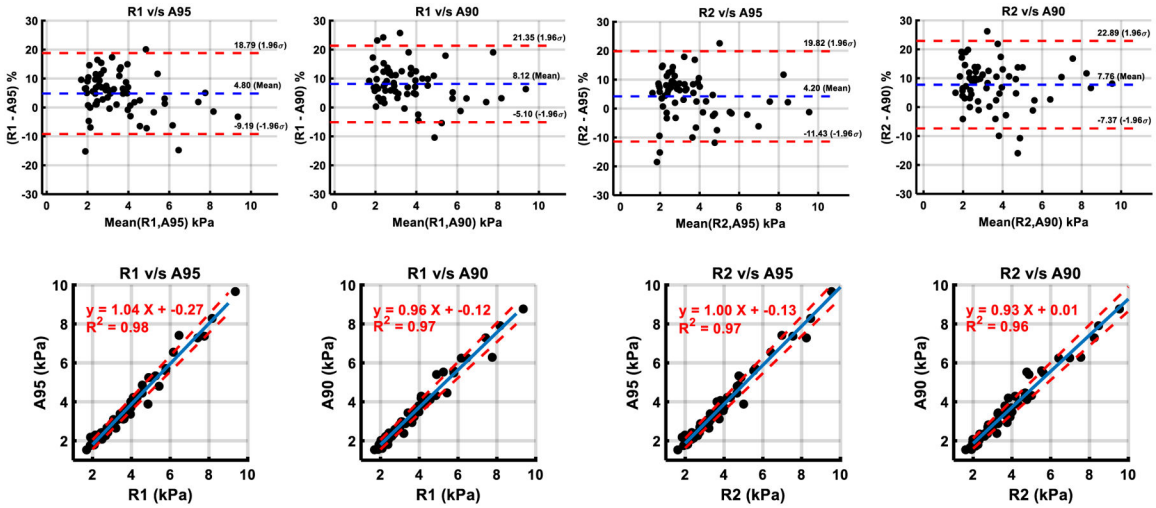


**Fig. 3.**

Comparison of shear stiffness measurements between manual and automated methods by Bland–Altman analysis and Linear Regression. Manual analysis informed by a 95% confidence mask by Reader 1 (R1) and Reader 2 (R2). Automated analysis using a 95% confidence mask (A95) and 90% confidence mask (A90). In scatter plots, blue line—list squares fit, dotted red line—95% confidence interval

**Table 1**

Comparison of area weighted liver shear stiffness values computed using manual and automated methods

| Region of interest analysis | Absolute difference (kPa) | Percent difference (%) | Fixed bias *p* value | Proportional bias, *p* value | ICC |
|---|---|---|---|---|---|
| R1,1-R1,2 | 0.04 ± 0.13 | 1.80 ± 2.75 | 0.231 | − 0.06, < 0.001 | 0.997 |
| R1-R2 | 0.01 ± 0.22 | 0.58 ± 5.02 | 0.657 | − 0.03, 0.044 | 0.992 |
| A95-A90 | 0.13 ± 0.28 | 3.24 ± 6.81 | < 0.001 | 0.07, < 0.001 | 0.988 |
| R1-A95 | 0.14 ± 0.28 | 4.80 ± 7.14 | < 0.001 | − 0.05, 0.017 | 0.988 |
| R1-A90 | 0.26 ± 0.28 | 8.12 ± 6.75 | < 0.001 | 0.03, 0.225 | 0.986 |
| R2-A95 | 0.13 ± 0.29 | 4.20 ± 7.97 | < 0.001 | − 0.02, 0.461 | 0.987 |
| R2-A90 | 0.27 ± 0.33 | 7.76 ± 7.72 | < 0.001 | 0.06, 0.017 | 0.982 |

Unless otherwise indicated, data are reported as the mean ± standard deviation. Manual analysis informed by a 95% confidence mask by Reader 1 (R1), and Reader 2 (R2). Automated analysis using a 95% confidence mask (A95) and 90% confidence mask (A90). Intra-reader comparison for a 95% confidence mask in 20 subjects using Reader 1's initial set of contours (R1,1) and his repeat contours (R1,2)

**Table 2**

Comparison of regions of interest by analysis methods

| Region of interest analysis | Absolute difference ($mm^2$) | Percent difference | Fixed bias *p* value | Proportional bias, *p* value | ICC |
|---|---|---|---|---|---|
| R1,1-R1,2 | − 602 ± 718 | − 33.1 ± 31.1 | < 0.001 | 0.19, 0.002 | 0.860 |
| R1-R2 | 20 ± 1054 | − 4.38 ± 43.8 | 0.766 | − 0.18, 0.003 | 0.615 |
| A95-A90 | − 795 ± 1064 | − 54.1 ± 113 | < 0.001 | − 0.44, < 0.001 | 0.608 |
| R1-A95 | 320 ± 1043 | 5.4 ± 41.2 | < 0.001 | 0.18, 0.014 | 0.497 |
| R1-A90 | − 475 ± 1298 | − 29.3 ± 66 | < 0.001 | − 0.31, < 0.001 | 0.471 |
| R2-A95 | 301 ± 1334 | − 4.1 ± 59 | < 0.001 | 0.42, < 0.001 | 0.314 |
| R2-A90 | − 495 ± 1577 | − 42.5 ± 93 | < 0.001 | − 0.127, 0.169 | 0.312 |

Unless otherwise indicated, data are reported as the mean ± standard deviation. Manual analysis informed by a 95% confidence mask by Reader 1 (R1), and Reader 2 (R2). Automated analysis using a 95% confidence mask (A95) and a 90% confidence mask (A90). Intra-reader comparison for a 95% confidence mask in 20 subjects using Reader 1's initial set of contours (R1,1) and his repeat contours (R1,2)

**Table 3**

Hepatic fibrosis classification performance by analysis methods

| Parameters for fibrosis classification | R2 | A95 | A90 | A95 | A90 |
|---|---|---|---|---|---|
| Cutoff value (kPa) | 2.27 | 2.27 | 2.27 | 2.21 (OPT) | 2.08 (OPT) |
| Sensitivity | (51/52) 98.08% | (45/52) 86.54% | (46/52) 88.46% | (49/52) 94.23% | (51/52) 98.08% |
| Specificity | (12/13) 92.31% | (12/13) 92.31% | (13/13) 100% | (12/13) 92.31% | (13/13) 100% |
| FP | 1 | 1 | 0 | 1 | 0 |
| FN | 1 | 7 | 6 | 3 | 1 |
| Accuracy | (63/65) 96.92% | (57/65) 87.69% | (59/65) 90.77% | (61/65) 93.85% | (64/65) 98.46% |

Clinical reference was manual analysis by Reader 1 (R1). Manual analysis informed by a 95% confidence mask by Reader 2 (R2). Automated analysis using a 95% confidence mask (A95) and a 90% confidence mask (A90)

*FP* false positive, *FN* false negative *OPT* optimal stiffness cutoff value for maximized sensitivity plus specificity